Applied Surface Science 635 (2023) 157598

Contents lists available at ScienceDirect

Applied Surface Science

journal homepage: www.elsevier.com/locate/apsusc

Full Length Article

Critical method evaluation refutes the Ar 2p signal of implanted Ar for referencing X-ray photoelectron spectra

G. Greczynski *, L. Hultman

Thin Film Physics Division, Department of Physics, Chemistry, and Biology (IFM), Linköping University, SE-581 83 Linköping, Sweden

ARTICLE INFO

Keywords:
XPS
Photoelectron spectroscopy
Ar 2p
Adventitious carbon
Charge correction
Calibration

ABSTRACT

Correct binding energy (BE) spectra referencing of insulating samples remains the major challenge in modern XPS analyses. Ar 2p signal of implanted Ar is sometimes used for this purpose. The method relies upon the assumption that chemically inert species such as noble gas atoms would be ideally suited as other factors affecting core level peak positions (such as chemical bonding) can be excluded. Here, we present a systematic study on the Ar 2p referencing method applied to a wide range of thin film sample materials of metals, nitrides, carbides, and borides. All specimens exhibit a well-defined Fermi edge, which serves as an independent internal reference for Ar 2p spectra of *in-situ* implanted Ar. Ar $2p_{3/2}$ binding energy is shown to vary by as much as 5.1 eV between samples. This is more than typical chemical shifts of interest, which obviously disqualifies Ar 2p referencing. The BE of the Ar 2p peaks shows a strong correlation to the number of valence electrons available for screening, implying that the polarization energy has a major role for the observed large spread of Ar $2p_{3/2}$ BE values. In several cases of single-phase films, an additional Ar 2p doublet is observed with the Ar $2p_{3/2}$ BE referenced to the vacuum level higher than the gas phase value of 248.6 eV, which is tentatively assigned to the formation of Ar-N and Ar-C complexes stabilized by Van der Waals forces. Ar implantation into two-phase samples, exemplified here by phase-segregated NiCrC/a-C:H and nanocomposite c-TiN/SiN_x thin films, leads to complex Ar 2p spectra, which further demonstrates unreliability of the referencing method. The firm conclusion of the study is that the Ar $2p_{3/2}$ peak from implanted Ar is not a remedy for the charge referencing problem.

1. Introduction

The virtue of XPS is its capability to study chemical bonding [1]. This is assessed directly from measured positions of spectral peaks on the binding energy (BE) axis that correspond to core level energies in atoms [2,3]. The latter are affected by the redistribution of valence charge during formation of chemical bonds, which allows to determine the type of bonds that are formed in the specimen. Peak positions are best defined for metallic samples, which make good electrical contact to the spectrometer resulting in a common Fermi level that serves as an internal reference [4–7]. Vast majority of chemical shifts in compound materials are to the higher BE with respect to the metal peak (i.e., negative charge density on metal atoms decreases as a result of bond formation). Unfortunately, peak shifts in the same direction can also occur if sample conductivity is not high enough to allow for replenishment of emitted electrons with sufficiently high rate, resulting in positively-charged surface [8]. Thus, a reliable internal reference (charge reference) is necessary for correct interpretation of peak shifts.

The most common method of referencing XPS spectra relies on the C 1 s signal from the contamination layer (adventitious carbon, AdC), which is detected essentially on all specimens except those made and analyzed *in-situ-vacui*. However, early-recognized problems with the C 1 s method, such as undefined chemical composition of the AdC layer [9], its unknown origin [10], and the arbitrarily defined position of the C 1 s peak [11–16], stimulated efforts towards finding alternative solutions. An interesting technique based on monitoring the signal from implanted noble gas atoms was proposed by Paterson et al. [17] for Auger electron spectroscopy and thereafter adopted for XPS by Kohiki et al.18 This approach relies on measuring core level lines of noble gas atoms (e.g., Ar $2p_{3/2}$ line of Ar) implanted in the host material to be analyzed, to the extent that the implantation does not significantly alter the sample of interest. The assumption made is that in the absence of chemical bonding between Ar atoms and actual elements present in the sample, the signal from noble atoms would only be affected by the local

* Corresponding author.
E-mail address: grzegorz.greczynski@liu.se (G. Greczynski).

https://doi.org/10.1016/j.apsusc.2023.157598
Received 17 March 2023; Received in revised form 22 May 2023; Accepted 23 May 2023
Available online 29 May 2023

electrical potential, hence, it would serve the purpose of perfect charge reference. The obvious advantage over the C 1 s/AdC method is that the reference signal comes from an element in the interior of the sample of interest (within XPS detection range) and not present as an external layer (such as AdC).

In their original experiments Kohiki et al. implanted 5 keV Ar^+ ions into several sample types that included Pd, Ag, and Au foils, as well as Si, SiO_2, and soda glass [18]. The charging condition for insulating samples was varied by altering the x-ray power and using flood gun with different settings. Authors observed that the Ar $2p_{3/2}$ signal of implanted Ar shifts together with all major peaks from the soda glass sample to within ±0.2 eV, which led them to the conclusion that the former peak can be used as the energy reference. The "correct" BE of the Ar $2p_{3/2}$ line was established at 241.5 ± 0.2 eV for metallic samples based on results for Pd, Fe, and graphite samples.

Markedly, the value recommended for insulators was, however, different at 242.3 eV. The reason for that is that the C 1 s peak of AdC on insulating sample was found at different (?!) BE than the corresponding signal on metals: 283.8 eV *vs*. 284.6 eV, respectively. Perhaps, authors could not resist the notion of a constant C 1 s BE and decided to *calibrate the Ar $2p_{3/2}$ peak position against that of the C 1 s peak of AdC* and ascribed this 0.8 eV shift to the difference in extra-atomic relaxation energy for Ar atoms implanted in conducting and insulating samples. That was done despite knowing about the C 1 s referencing issues as proven by extensive discussion of that topic in the very same paper [18]. The verification of the spectra referencing to the Ar $2p_{3/2}$ peak set at 242.3 eV was then done by comparing obtained positions of Si 2p peaks from soda glass and SiO_2 samples to previously reported values. An agreement within ±0.4 eV was found, which at that time could be regarded satisfactory (the instrument used provided FWHM of the Ag $3d_{5/2}$ peak equal to 1.1 eV, while modern spectrometers give values of 0.5 eV or better). The same accuracy was concluded in the follow-up paper [19], in which the same group applied the method to insulating materials with varying bond ionicity: BN, GaP, InP, BeO, and NaCl. Although it was not explicitly stated where the C 1 s peak was found for these samples, authors write that the procedure was the same as in the first paper. Authors consider the extra-atomic relaxation energy to be constant for all metals such that the Ar $2p_{3/2}$ peak is shifted by 2.5 eV with respect to the gas phase value. The corresponding shift for insulators was prescribed as 1.7 eV.

The papers by Kohiki et al. [18,19] on the Ar $2p_{3/2}$ referencing neglected to some extent earlier results of Citrin et al. [20] who demonstrated already in 1974 that the BE of the Ar 2p peak depends on the host material. In that work 1 keV noble gas ions were implanted into Cu, Ag, and Au. Ar $2p_{3/2}$ line for Cu, Ag, and Au host was found at 241.1, 241.2, and 240.3 eV, respectively (all values given with respect to the Fermi level). At that time the main concern was the comparison to the gas phase values to pinpoint mechanism responsible for observed lower BE values in solids, considering extra and intra-atomic relaxation as well as chemical effects resulting from compression of outer electron wave functions upon implantation into solid (leading to stronger Coulomb interaction between outer and inner electrons and, thus, reduced core level binding energy) [21,22]. The dominant effect responsible for the peak shift was concluded to be the differences in polarization energy (or core hole screening) between host materials. Our results presented in Sec. 3.2 fully support this interpretation.

An apparent advantage of Ar $2p_{3/2}$ referencing would be that Ar^+ sputter guns are available on all XPS instruments providing easy means of Ar implantation (intentional or not) in samples to be analyzed. For an incident energy in the range 1–5 keV, the implantation depth largely also overlaps with the XPS probing depth. One thing to consider, however, is the possibility of sputter damage in the top surface layer, which scales with the Ar^+ energy and, in the worst case, can lead to that the layer where Ar is implanted is not representative of the pristine material to be studied [23–25]. The actual implantation of Ar can also give rise to forward sputtering and Frenkel pair formation, where the resulting lattice point defects may affect the bonding signatures of the studied material.

Ar $2p_{3/2}$ referencing could also be seen as a good alternative for, e.g., sputter depth profiles as in such case Ar is present "by default", while other referencing techniques such as, e.g., noble metal decoration are not practical to implement (would require depositing new noble metal layer after each etching step).

Shortly after the Ar $2p_{3/2}$ method was introduced, Church et al. complemented the noble gas referencing technique by demonstrating that, as the surface charge changes, the peaks of implanted Xe atoms shift together with other signals from the sample, while the Auger parameter remains constant [26]. This observation established that, indeed, signals from noble gas atoms can be used to monitor surface potential. Noble Ar referencing was later confirmed to serve well in studies of several oxides such as γ-Al_2O_3, ZrO_2, SiO_2, and Y_2O_3 [27]. In those experiments, the Ar $2p_{3/2}$ peak of implanted Ar was found at 242.3 ± 0.1 eV, while referenced to the Au $4f_{7/2}$ peak of evaporated Au that was set at 84.0 eV. Much larger variation was found in the position of the C 1 s peak of adventitious carbon, which was measured anywhere between 284.1 and 284.9 eV (!), depending on the sample (values also referenced to the Au $4f_{7/2}$ line at 84.0 eV). In any case, the above work assumes that the evaporated Au is in electrical equilibrium with the host material, an assumption that already at that time was questionable [28,29]. Another reservation to results reported in Ref. 27 was revealed in later studies that demonstrated the shift in Au $4f_{7/2}$ line as a function of cluster size [30,31]. In addition, the very different photoelectron current from Au clusters as compared to the matrix material also disqualifies Au referencing [32].

Ar signal was also used for referencing XPS spectra in cases where the C 1 s method gave confusing results [33] or the AdC layer was not available [34–39]. It must be emphasized though that, except for the paper by Pelisson-Schecker et al. discussed below in more detail, the Ar $2p_{3/2}$ method was applied in those papers with no parallel verification for correctness of results.

Further problems with Ar referencing were reported by Pelisson-Schecker et al. who used XPS to analyze a series of Al-Si-N samples deposited by magnetron sputtering [33]. It was found that the Ar $2p_{3/2}$ peak shifts with varying Si content by as much as 1 eV with respect to the Au $4f_{7/2}$ line from deposited Au clusters. The shift was correlated with a rapid increase in the concentration of trapped Ar atoms. This result was associated with an observed change in the Ar Auger parameter, calculated as the sum of the kinetic energy of the Ar(LMM) Auger line and the binding energy of the Ar $2p_{3/2}$ peak, and interpreted in terms of preferential Ar location at grain boundaries leading to large chemical shifts. Once should also consider that Au and Si peaks may be affected by their mutual phase solubility and tendency of Au to catalyze oxidation of Si [40–42]. In addition, conductivity in the phase where Ar is being implanted may very well be a function of the Ar concentration. Nevertheless, this and examples above show that the noble character of implanted atoms does not guarantee constant binding energy, hence they cannot serve as a reliable BE reference.

As evident from the literature survey presented above, spectra referencing to the Ar $2p_{3/2}$ line of implanted Ar gave mixed results over the last 40 years, since the time the method was first proposed. Here, we present a systematic study aiming to test the reliability of this charge referencing method. We follow the same approach as employed previously for testing the C 1 s technique [15], i.e., using a series of metallic samples all of which feature an independent internal reference in the form of a well-defined Fermi edge. This procedure ensures that following *in-situ* Ar implantation, the measured Ar $2p_{3/2}$ peak positions can be directly referenced to the spectrometer Fermi level. The metallic character of all specimens (with the exception of SiN, which is used only as a reference in Sec. 3.4) and adequate sample mounting eliminates the risk of surface charging. A reasonably constant value of Ar $2p_{3/2}$ BE is expected under such conditions if that signal would have the merit of a reliable charge reference.

2. Experimental details

All specimens used in the study are in the form of thin films grown by dc magnetron sputtering on Si(001) substrates. Metallic films include Al, Ag, Au, Co, Cr, Cu, Fe, Hf, Mn, Nb, Ni, Pt, Sc, Ti, V, Y, and Zr, while compound samples are TiB_2, ZrB_2, VN, VC, ZrN, ZrC, CrN, CrC, HfC, HfN, TiN, TiC, NbC, NbN, NiCrC, TiSiN, and SiN (the only insulator in the sample set added as a reference to the case study presented in Sec. 3.4). An industrial-size CC800/9 CemeCon AG system with the base pressure lower than 2.3×10^{-6} Torr (0.3 mPa) is used (except for the NiCrC growth, which is discussed separately in Sec. 3.4). Deposition of metallic, boride, and carbide samples is conducted in Ar, while Ar/N_2 gas mixture (with the N_2–to-Ar flow ratio optimized to obtain stoichiometric single-phase layers) is used for the nitride growth. Elemental targets are used for deposition of metallic and nitride samples. Boride films are grown from rectangular 8.8×50 cm^2 compound targets, while carbides are grown in co-sputtering geometry using elemental and graphite targets. The total pressure during all depositions is kept constant at 3 mTorr (0.4 Pa). Si(001) substrates previously cleaned in acetone and isopropanol are biased at −60 V and mounted 18 cm away from the target surface. The average target power is set at 2 kW, while the resulting film thickness ranges from 140 to 720 nm. The heating is accomplished with two resistive heaters operating at 8.8 kW each, ensuring the substrate temperature of 470 ± 10 °C. In order to minimize the influence of venting temperatures on the surface oxide layer thickness [43], all specimens are allowed to cool down to RT before exposure to the laboratory atmosphere.

XPS analyses are performed in an Axis Ultra DLD instrument from Kratos Analytical (UK) with the base pressure during spectra acquisition better than 1.1×10^{-9} Torr (1.5×10^{-7} Pa), achieved by a combination of turbomolecular and ion pumps. Monochromatic Al Kα radiation ($h\nu = 1486.6$ eV) is used with the anode power set to 150 W. All spectra are collected at normal emission angle. The analyzer pass energy is 20 eV, which yields the full-width-at-half-maximum (FWHM) of 0.55 eV for the Ag $3d_{5/2}$ peak. Ar^+ beam is incident at 20° from the surface plane. The ion energy is either 0.5, 1, or 4 keV (as specified below), while the etching time is 10, 6, and 2 min, respectively. Witch each setting the steady state situation is reached, i.e., the spectra appearance does not change any more with further etching. The total Ar ion dose is in the range from 0.94×10^{17} to 1.26×10^{17} cm^{-2}. The sample area etched by the ion beam is 3×3 mm^2, while the analyzed area is 0.3×0.7 mm^2. Spectrometer binding energy scale is calibrated according to the ISO standards for monochromatic Al Kα sources that place Au $4f_{7/2}$, Ag $3d_{5/2}$, and Cu $2p_{3/2}$ peaks at 83.96, 368.21, and 932.62 eV, respectively [44]. All core-level spectra are charge-referenced to the Fermi edge cutoff, which results in core level peak positions that agree to within ±0.1 eV with those from XPS hand books [45]. Spectra deconvolution and quantification is performed using CasaXPS software package (version 2.3.16) and sensitivity factors supplied by the instrument manufacturer [46]. Shirley background function and Voigt-type peak shapes are used. Asymmetrical peak shapes are fitted using Voigt functions (30% Gaussian-70% Lorentzian) convoluted with exponential tail functions [47]. The $2p_{3/2}$ to $2p_{1/2}$ peak area ratio is constrained at 2:1 for all Ar 2p doublets, while the energy splitting is allowed to vary between 2.1 and 2.2 eV. Sample work function ϕ_{SA} is obtained from ultraviolet photoelectron spectroscopy (UPS) measurements performed in the same instrument (immediately after XPS analyses to ensure that the surface is in the same state) with unmonochromatized He I radiation ($h\nu = 21.22$ eV) and a −10 V bias applied to the sample stage. ϕ_{SA} is assessed from the secondary-electron cutoff energy in the He I UPS spectra by a linear extrapolation of the low-kinetic-energy electron tail towards the BE axis [48,49]. For the sputter-etched reference Au sample, $\phi_{SA} = 5.30$ eV, in very good agreement with the textbook values that range from 5.0 to 5.4 eV [48].

3. Results and discussion

3.1. Ar 2p spectra from thin film samples irradiated with 4 keV Ar^+

Fig. 1 shows a set of Ar 2p spectra recorded from Al, Ag, Au, Cr, Cu, Fe, Mn, Pt, Sc, Ti, V, and Y thin film metal samples after 2 min etching with 4 keV Ar^+ ions incident at a shallow angle of 20° from the surface plane (see Supplementary file for corresponding survey and major core level spectra). These results are selected out of all data recorded from seventeen metallic films, as the most representative to be discussed below. Also shown are the corresponding valence band spectra recorded in the vicinity of the Fermi level (FL) to verify that samples are in good electrical contact to the spectrometer. Fig. 2 displays Ar 2p spectra from selected compound thin film samples with well-defined FL including TiB_2, ZrB_2, VN, ZrN, TiN, and TiC (survey and major core level spectra shown in the Supplementary file). This small subset, selected out of fifteen compound thin film specimens that are included in the study (for other spectra see Secs. 3.3 and 3.4 together with related figures), serves here as representative example of spectra complexity. Clearly, both the spectral shape and, most importantly, the peak position, exhibit large dependence on the sample type. In some cases (Ag, Al, Cr, Cu, Fe, Mn, TiB_2, and TiC) spectra show the evidence for two spin-split doublets (see Sec. 3.3). The peaks width also varies considerably between samples.

The most important observation in the context of this paper is that *the BE of the Ar $2p_{3/2}$ peak varies by as much as 5.1 eV with respect to the sample Fermi level for the different samples*. The lowest Ar $2p_{3/2}$ BE is measured for Pt (240.3 eV) followed by Au (240.9 eV), Ag, Cu, and TiB_2 (all at 241.7 eV). The highest value is measured for Ar implanted in the TiN sample, in which case doublets are observed with Ar $2p_{3/2}$ peaks at 245.4 eV and 243.1 eV (see Sec. 3.3 and Fig. 4 (d)-4(f)). Ar 2p doublets shifting to very high BE are also noted for Ar implanted in HfC (Ar $2p_{3/2}$ at 245.2 eV), ZrC (245.1 eV), TiC (244.7 eV), and VN (244.4 eV). In the group of samples that show single pair of $2p_{3/2}$-$2p_{1/2}$ peaks, the highest Ar $2p_{3/2}$ BE is observed for Ti (243.1 eV) and Zr (243.0 eV).

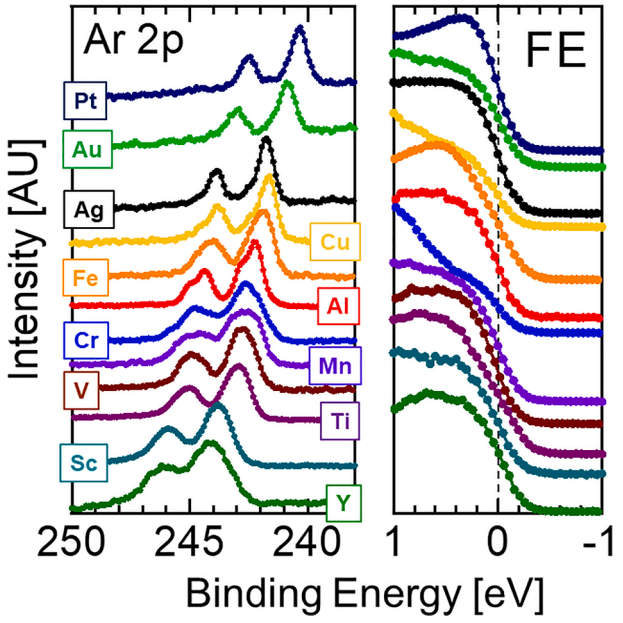

Fig. 1. (left) Ar 2p spectra recorded from Al, Ag, Au, Cr, Cu, Fe, Mn, Pt, Sc, Ti, V, and Y thin film samples after 2 min etching with 4 keV Ar^+ ions incident at an angle of 20° from the surface plane. (right) corresponding spectra recorded in the vicinity of the Fermi level. The position of the Fermi edge (FE) serves as an internal energy reference.

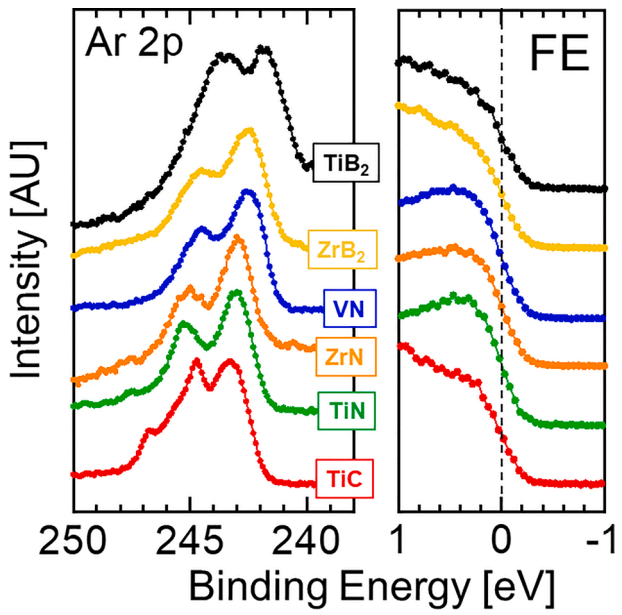

Fig. 2. (left) Ar 2p spectra for selected compound thin film samples: TiB_2, ZrB_2, VN, ZrN, TiN, and TiC. (right) corresponding spectra recorded in the vicinity of the Fermi level. The position of the Fermi edge serves as an internal energy reference.

3.2. *Ar $2p_{3/2}$ peak shifts*

The Ar $2p_{3/2}$ peak positions for the 31 thin film samples (17 metals and 14 compounds) irradiated with 4 keV Ar^+ ions spanning various materials systems (metals, nitrides, carbides, and borides) are presented in Fig. 3 (a). In all cases a well-defined FL is used as an internal charge reference (for that reason the SiN sample is excluded here). In the case of complex spectra two values are given based on the rigorous peak fitting. Out of the entire sample set only in four cases the Ar $2p_{3/2}$ peak is reasonably close to the "reference" position of 241.5 eV proposed in Ref. 18 for metallic samples. Those are Ag, Cu, and TiB_2 all featuring Ar $2p_{3/2}$ peak at 241.7 eV as well as Ni with the Ar $2p_{3/2}$ peak at 241.4 eV. In all other cases, depending on the sample, the Ar $2p_{3/2}$ peak shifts in both directions from the "reference" value. The largest deviation to the low BE side is 1.2 eV for Pt film. However, for the vast majority of samples (28 out of 31 tested) Ar $2p_{3/2}$ peak is observed at the BE higher than 241.5 eV. In the extreme case the deviation to the high BE side is as large as 3.9 eV (TiN). *Such large peak shifts between various sample types obviously disqualify Ar $2p_{3/2}$ peak as a charge reference.* The apparent "match" for Ag, Cu, and TiB_2 appears to be a coincidence rather than the rule.

A clear trend is observed in the position of the Ar $2p_{3/2}$ peak for row one and two transition metals. The peak from implanted Ar shifts gradually towards lower BE with increasing the column number in the periodic table: from 243.8 eV for Sc (column III), to 243.1 eV for Ti, 242.8 eV for V, 242.3 eV for Cr and Mn, thereafter to 242.1, 241.7, 241.4, and 241.6 eV for Fe, Co, Ni, and Cu (column XI), respectively. *Thus, the BE of the Ar 2p peaks shows a strong correlation to the number of valence electrons available for screening, which means that the polarization energy has a significant role for the observed large spread of Ar $2p_{3/2}$ BE values* (2.4 eV for the discussed sample subset). Analogical trend is also observed for row 2 metals (Y, Zr, Nb, and Ag) with the Ar $2p_{3/2}$ peak shifting from 244.1 eV for Y (column III) to 241.7 eV for Ag (column XI). Not enough data is available for the row 3 TMs due to the overlap of Ar 2p peaks with Ta 4d and W 4d core levels.

Trends outlined above are, to some extent, present also for TM ceramic compound samples. Considering lower BE Ar 2p doublets only (see Sec. 3.3), the Ar $2p_{3/2}$ peak shifts from 243.3 eV for TiC, to 242.5 and 241.9 eV for VC and CrC, respectively, thus following the same order as for parent metals. Similarly, Ar $2p_{3/2}$ peak is at 243.1 eV for TiN, 242.6 eV for VN, and 241.9 eV for CrN.

In Fig. 3(b) Ar $2p_{3/2}$ BE values are replotted with respect to the sample vacuum level (VL) after obtaining work function values by UPS

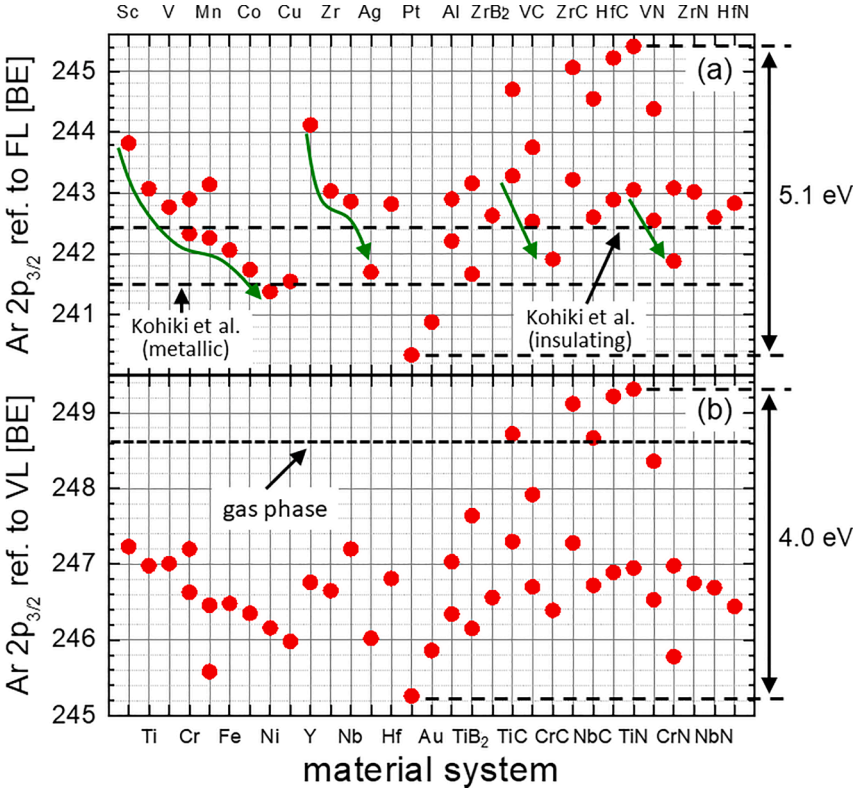

Fig. 3. (a) Ar $2p_{3/2}$ peak positions for 31 thin film samples (17 metals and 14 compounds) irradiated with 4 keV Ar^+ ions spanning various materials systems (metals, nitrides, carbides, and borides). In all cases a well-defined FL is used as an internal charge reference (for that reason the SiN sample is excluded here). Two values given for some samples mean that Ar 2p spectra are composed of two doublets. (b) the Ar $2p_{3/2}$ peak positions referenced to the vacuum level (VL, using the work function values obtained by UPS from the Ar^+-etched surfaces). Green arrows indicate that the Ar $2p_{3/2}$ peak positions correlate to the number of valence electrons. (For interpretation of the references to colour in this figure legend, the reader is referred to the web version of this article.)

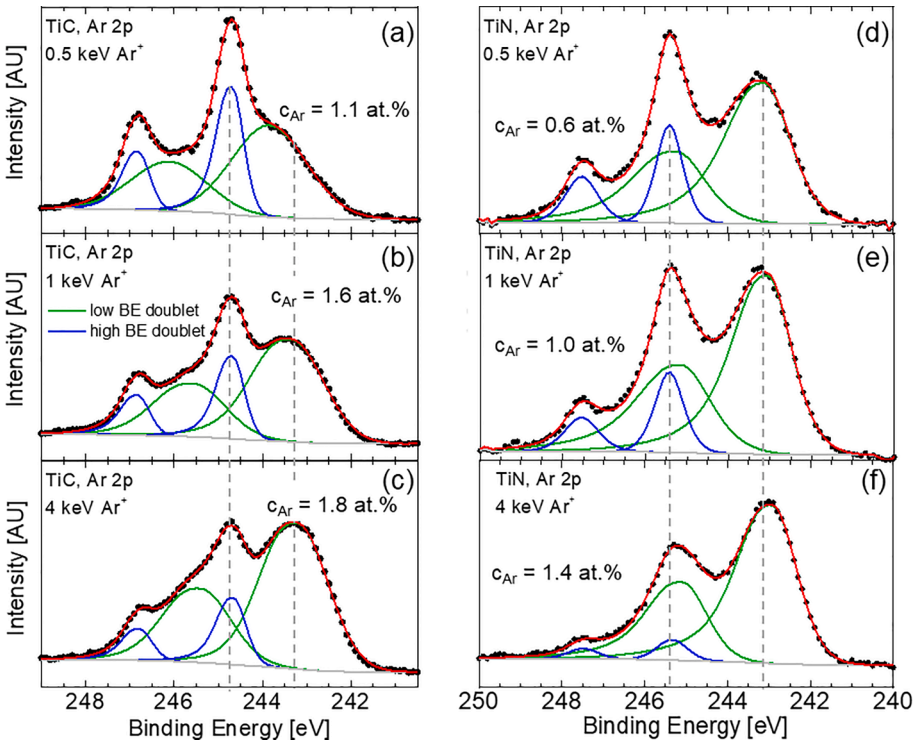

Fig. 4. Ar 2p spectra as a function of Ar^+ incident energy varied from 0.5 to 4 keV for (a)-(c) TiC and (d)-(f) TiN thin film samples. Ar concentrations are derived from XPS quantitative analysis.

from the surfaces etched with 4 keV Ar^+ ions. Also in this case, the spread between the lowest and the highest value is very large: the position of the Ar $2p_{3/2}$ peak varies by 4.0 eV, from 245.3 eV for Pt to 249.3 eV for the higher BE peak from Ar implanted in TiN. Interestingly, in five cases the measured Ar $2p_{3/2}$ BE is higher than the gas phase value of 248.6 eV [10]. These are TiN, HfC, ZrC, TiC, and NbC with the peaks at 249.3, 249.2, 249.1, 248.8, and 248.7 eV, respectively. This is very surprising as Ar 2p BE's should always be lowered once Ar is implanted

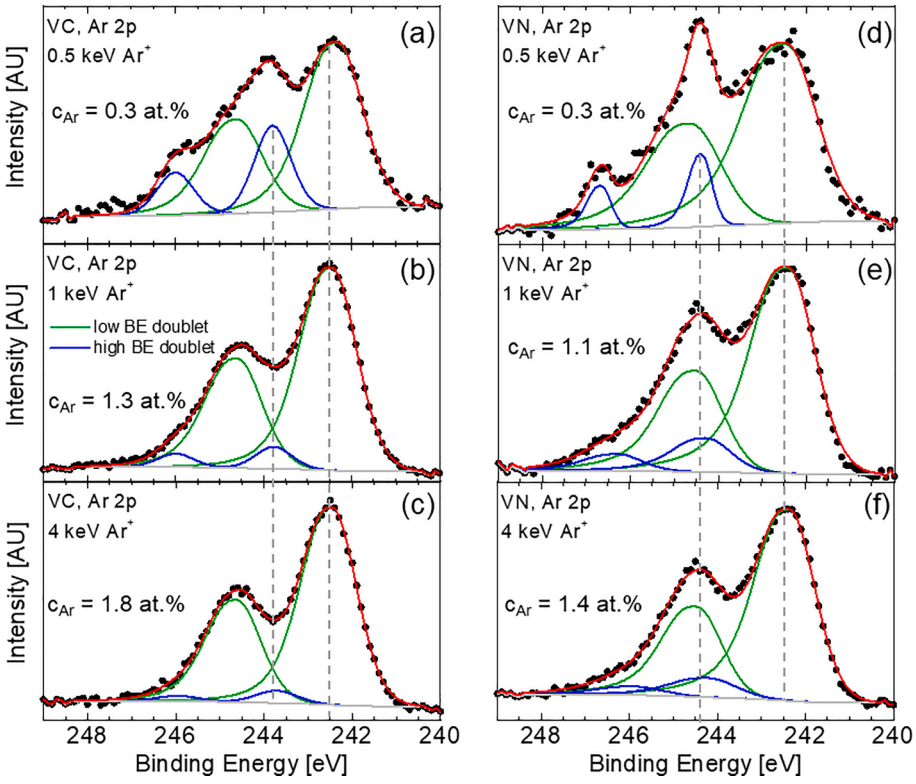

Fig. 5. Ar 2p spectra as a function of Ar^+ incident energy varied from 0.5 to 4 keV for (a)-(c) VC and (d)-(f) VN thin film samples. Ar concentrations are derived from XPS quantitative analysis.

in a solid due to the screening response from the host material [20-22]. To the best of our knowledge this is the first time such high BE values are reported for Ar implanted in solid state samples. In all these samples two Ar 2p doublets are observed although the thin film specimens are homogenous single-phase materials (more complex materials are discussed in Sec. 3.4).

In several other samples, which show two Ar 2p doublets, the Ar $2p_{3/2}$ BE is also very high (although not exceeding the gas phase value). These are VN (248.4 eV), VC (247.9 eV), and TiB_2 (247.6 eV). Other values are significantly lower - TiC (lower BE peak at 247.3 eV), Cr (higher BE peak at 247.2 eV), followed by Ti, V, and TiN (all at 247.0 eV). The lowest value is obtained for Pt (245.3 eV), followed by Mn (lower BE peak at 245.6 eV), Au (245.9 eV), Ag (246.0 eV), and Cu (246.1 eV). Thus, the maximum shift to lower BE with respect to the gas phase value is 3.3 eV for Ar implanted in the Pt sample.

Our values of 241.7 eV for Ar implanted in Cu and Ag, and 240.9 eV if Au is used as a host material compare very well to those reported by Citrin et al, who also used FL referencing and found Ar $2p_{3/2}$ peaks at 241.1, 241.2, and 240.3 eV, respectively [20]. Thus, the same relative shifts are observed between samples while the absolute values are higher by 0.6 eV in our case.

3.3. The effects of Ar^+ incident energy

Figs. 4-6 illustrate the evolution of Ar 2p spectra from the first row Group IVB-VIB transition metal carbide and nitride thin film samples, i.e., TiC, TiN, VC, VN, CrC, and CrN (see Supplementary file for corresponding survey and major core level spectra). For all specimen types, the incident Ar^+ energy is varied from 0.5 to 4 keV. Concentrations of implanted Ar derived from XPS are also given in the figures. Markedly, CrC is the only case where spectra can be satisfactory fitted with a single $2p_{3/2}$-$2p_{1/2}$ doublet (cf. Fig. 6(a)-(c)). For all other films, a second doublet shifted to higher BE is necessary.

Two Ar 2p doublets were reported previously [50] upon implantation of 4 keV Ar^+ into sputtered Al film. In those works, the low BE Ar $2p_{3/2}$ peak was detected at 242.0 eV (we measured 242.2 eV – not shown here) and assigned to Ar in interstitials and/or small gas bubbles. The higher BE component was shifted by 0.75 eV (*vs.* 0.73 eV in our case) and assigned to Ar in larger bubbles. This assignment was supported by an increase in the intensity of the high BE peaks with increasing Ar^+ energy, which was previously associated with the formation of larger bubbles [51]. The BE of the Ar $2p_{3/2}$ peak was also found to increase with annealing temperature, which was explained by the bubbles growing by coalescence: the larger the bubble size the poorer screening of core holes created on Ar atoms within such bubbles by conducting electrons [52,53].

Markedly, the extra Ar 2p peaks, marked as "high BE doublets" in Figs. 4–6, best visible in spectra from TiC and TiN films irradiated with 0.5 keV Ar^+, have a number of peculiar features that make them distinctly different from the case of Ar-implanted Al samples described above. Those features are: (a) the Ar $2p_{3/2}$ BE is very high, up to 245.4 eV, which is, to the best of our knowledge, ca. 2–3 eV higher than any values reported before for solid state samples (e.g., the higher BE Ar $2p_{3/2}$ peak from Ar implanted in Al is at 242.93 eV), (b) the intensity of the high BE doublet decreases with increasing Ar^+ energy (opposite effect to what is observed for gas bubble formation), (c) the FWHM of the high BE doublet is very low, e.g., in the case of spectra from TiC films only 0.6–0.7 eV *vs.* 1.9–2.0 eV for low BE Ar 2p peaks, (d) energy splitting between low and high BE Ar 2p peaks is larger for nitrides, (e) the intensity ratio between low and high BE Ar 2p doublets show no dependence on the sample tilt angle.

All features listed above point towards different origin of high BE Ar 2p doublets shown in Figs. 4–6 (marked as "high BE doublets") than gas bubble formation. Such large shift can result from (1) a chemical effect or (2) a spectroscopic effect. The first explanation may seem counter-intuitive as Ar being a noble element is commonly considered not

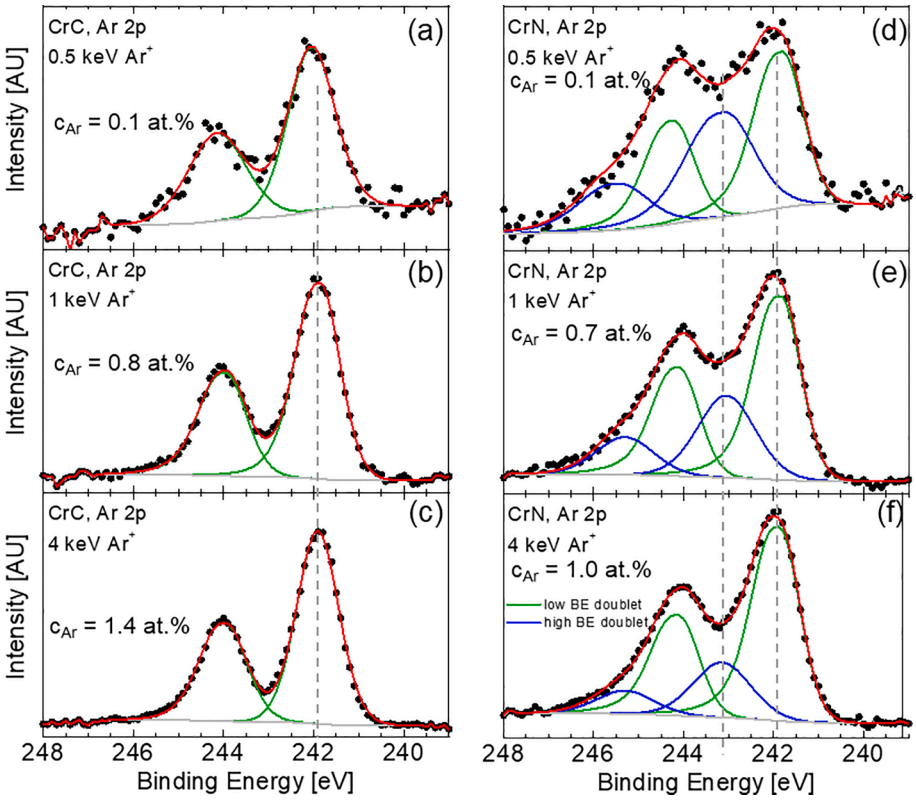

Fig. 6. Ar 2p spectra as a function of Ar^+ incident energy varied from 0.5 to 4 keV for (a)-(c) CrC and (d)-(f) CrN thin film samples. Ar concentrations are derived from XPS quantitative analysis.

partaking in chemical bonding. It can, however, bind weakly to other atoms and form Van der Waals molecules [54], such as C-Ar (Ref. [55]) or B-Ar [56]. Thus, one possible interpretation of high BE Ar 2p peaks shown in Figs. 4–6 is the formation of Ar-C (or possibly Ar-N) complexes. An alternative explanation involves spectroscopic effect such as, for example, poorly screened final state of the type observed for Ti 2p core levels of TiN [57–59], ZrN, VN, and HfN [60].

A clue may be the observation that lower BE Ar 2p peaks grow in intensity with increasing Ar concentration (achieved here by means of using higher Ar^+ energy), while the higher BE doublets remain unchanged. This is best seen in Figs. 7 and 8, where Ar 2p spectra from TiC, VC, CrC, TiN, VN, and CrN are plotted after normalization to the corresponding 2p signals. In the case of carbides Ar $2p_{3/2}$ peaks shift from 243.3 eV for TiC to 242.5 eV for VC and 241.9 eV for CrC. Similarly, for nitride samples, the Ar $2p_{3/2}$ peaks are at 243.1, 242.6, and 241.9 eV for TiN, VN, and CrN, respectively. Both trends can be explained by an increased core hole screening as the number of valence electrons on the parent metal increases from Ti to Cr.

C 1 s spectra from TiC, VC, and CrC samples are shown in Fig. 9. Markedly, in the case of TiC and VC films just one peak is observed indicating that specimens do not contain a second phase of amorphous carbon often encountered in transition metal carbides grown by magnetron sputtering [61]. Thus, the interpretation of two doublets in

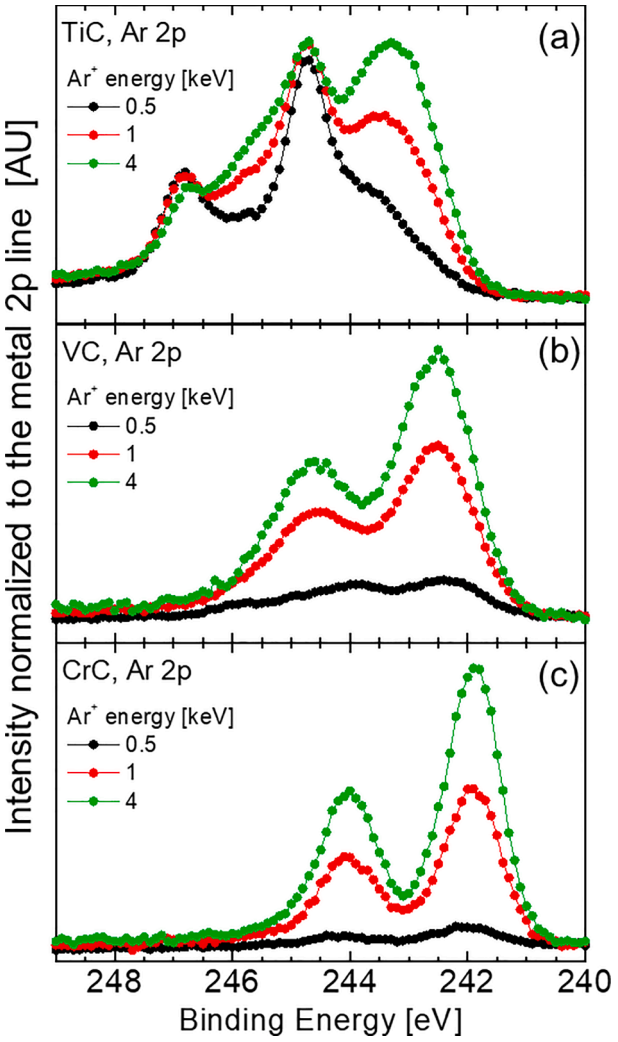

Fig. 7. Ar 2p spectra from (a) TiC, (b) VC, and (c) CrC thin film samples. In each case result after etching with 0.5, 1, and 4 keV Ar^+ ions are shown. To facilitate comparison, spectra are normalized to the intensity of corresponding 2p metal lines.

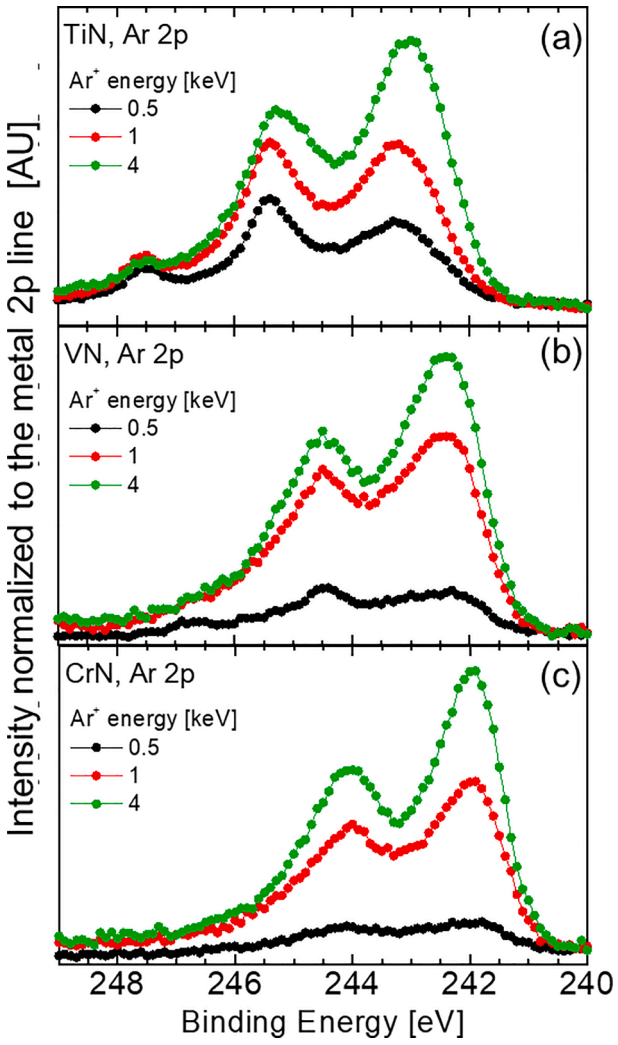

Fig. 8. Ar 2p spectra from (a) TiN, (b) VN, and (c) CrN thin film samples. In each case result after etching with 0.5, 1, and 4 keV Ar^+ ions are shown. To facilitate comparison, spectra are normalized to the intensity of corresponding 2p metal lines.

Ar 2p spectra in terms of sample inhomogeneity (Ar implanted in different phases with different conductivity gives rise to two doublets) can be excluded. Interestingly, C 1 s spectrum from the CrC film shows more complex structure, especially if lower Ar^+ energy is used for etching (cf. Fig. 9(c)), however in this case Ar 2p spectra show only one doublet.

The second (high BE) doublet is also observed in Ar 2p spectra recorded from ZrC and HfC (see Fig. 10(a) and 10(c)), although the signals are to some extent obscured by the inelastic background from Zr 3d and Hf 4d core levels. The BE of Ar $2p_{3/2}$ peak of that doublet is very high at 245.1 and 245.2 eV for ZrC and HfC, respectively. Interestingly, the high BE doublets are absent in Ar 2p spectra from corresponding nitrides, i.e., ZrN and HfN (cf. Fig. 10(b) and 10(d)), which is in contrast to the TiC-TiN pair.

Irrespective of the actual cause of the high BE Ar 2p doublet, determination of which is outside the scope of this paper, its presence further complicates the idea of using Ar $2p_{3/2}$ peaks as a charge reference.

3.4. Ar implanted in thin film samples with non-homogenous structure

As demonstrated in the previous sections, BE of Ar 2p doublets varies in a wide range depending on the material type. In many cases, two Ar

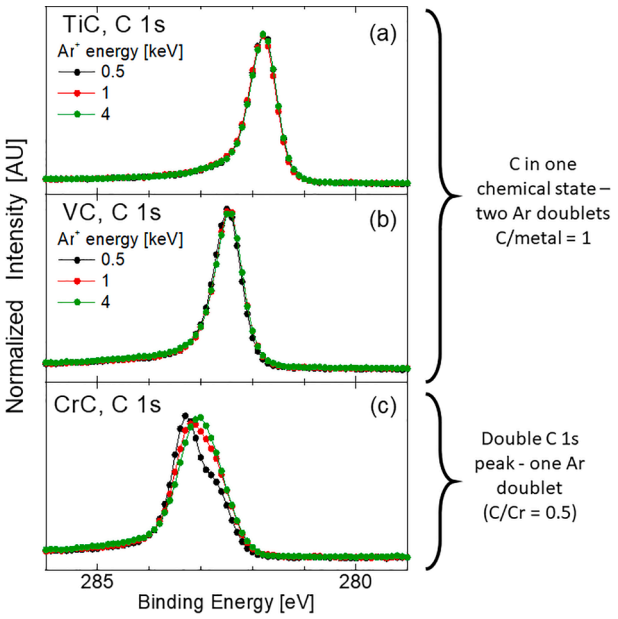

Fig. 9. C 1 s spectra from (a) TiC, (b) VC, and (c) CrC thin film samples. In each case result after etching with 0.5, 1, and 4 keV Ar^+ ions are shown. To facilitate comparison, spectra are normalized to the maximum intensity.

2p doublets are observed even for single-phase films. Yet another degree of complexity is introduced if non-homogenous samples are analyzed. In this section we discuss systems that represent the complexity often encountered in modern materials. The interpretation of Ar 2p spectra is supported by electron microscopy images. Results reveal clear dependence of the Ar 2p BE on where (i.e., in which phase) in the film the Ar atom is.

Fig. 11(a)-(i) illustrate the case of Ar implantation in NiCrC/a-C:H thin films deposited by pulse magnetron sputtering from an NiCr20 alloy cathode in Ar/C_2H_2 gas mixture [62]. With increasing carbon content, the segregation of the amorphous carbon was observed followed by self-assembly resulting in nanostructures consisting of metallic columns (3–7 nm in diameter) surrounded by carbon tissue phase, with axes parallel to the growth direction and thickness dependent on the C content. Fig. 11(a)-(c) show Ar 2p spectra recorded after 10 min. sputter-etching with 0.5 keV Ar^+ ions from samples containing 21, 48, and 63 at. % C, while the corresponding TEM images are displayed in Fig. 11(d)-(f). C 1 s spectra displayed in Fig. 11(g)-(i) further prove that the films are two-phase composed of amorphous C (with the C 1 s peak from C-C/C–H bonds at 284.4 eV) and carbide phase (C 1 s peak at 283.1 eV).

In the case of NiCrC/a-C:H film with the C content of 21 at.%, the structure is nearly homogenous (cf. Fig. 11(d)) with vast majority of C atoms bonding to metals, as evidenced by the C 1 s spectrum in Fig. 11 (g) [62]. In this case, also the Ar 2p spectrum exhibits single $2p_{3/2}$-$2p_{1/2}$ doublet with the $2p_{3/2}$ component at 241.1 eV assigned to Ar implanted as interstitial in the crystalline metal carbide grains. With increasing C content, films become two-phase as revealed by plan view TEM images (Fig. 11(e)-(f)), which results in that a second pair of Ar 2p peaks, shifted by 0.8 eV to higher BE, is observed after Ar implantation (Fig. 11(b)-(c)). The correlation between the relative intensity of the second Ar 2p doublet and the amount of the amorphous C phase (assessed by both TEM and corresponding C 1 s spectra) allows to assign the high BE peaks to Ar implanted in the amorphous phase. The measured Ar $2p_{3/2}$ BE of 241.9 eV agrees very well to that reported in Ref. [63] for the Ar in amorphous carbon film. In the case of the sample with the highest C content of 63 at.%, the high BE Ar 2p doublet assigned to Ar in the amorphous C dominates completely.

The 0.8 eV difference in BE between Ar 2p peaks from two phases, likely being the result of different screening ability of conduction electrons, illustrates the problem of using the Ar $2p_{3/2}$ signal for BE referencing. Aligning the spectra from the sample with the lowest and the highest C content to the maximum of the Ar $2p_{3/2}$ peak would (either way) result in the 0.8 eV error. The latter would be manifested by the inconsistent positions of core level peaks (e.g., carbide and amorphous carbon C 1 s peaks BE varying with C content in the sample) and by the sample Fermi edge not coinciding with the 0 eV on the BE scale.

Another example of Ar implantation in two-phase material systems is shown in Fig. 12(a)-(k). Ar 2p spectra acquired from four thin film samples sputter-etched with 4 keV Ar^+ ions are shown for: (a) a reference single-phase cubic TiN film, (b) a nanocomposite $Ti_{0.74}Si_{0.26}N$ film consisting of cubic-structure TiN-rich crystallites embedded in the SiN_x tissue phase, (c) single-phase cubic-structure $Ti_{0.76}Si_{0.24}N$ film, and (d) a reference SiN film [64]. Spectra in Fig. 12(a)-(c) are referenced to the Fermi edge, while for referencing the Ar $2p_{3/2}$ spectrum from the SiN

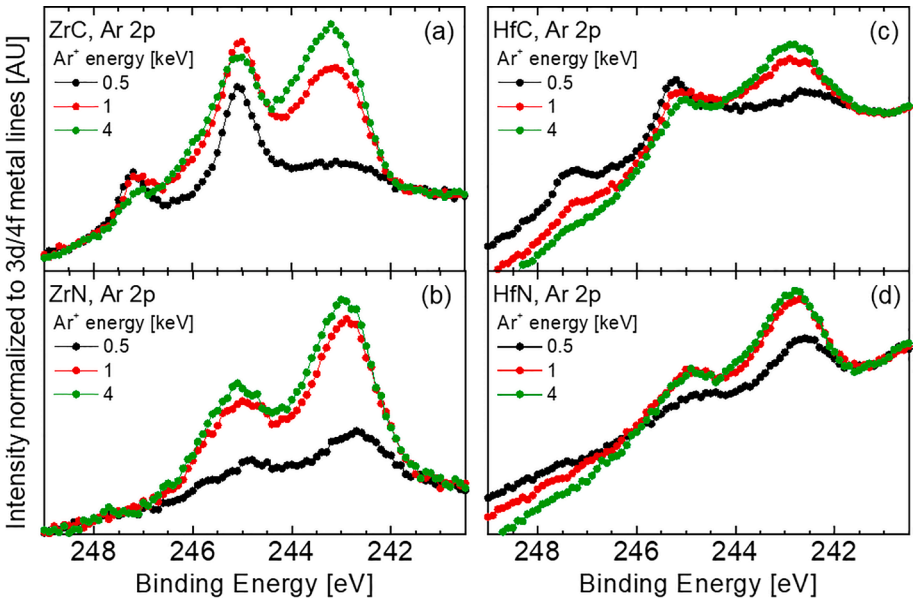

Fig. 10. Ar 2p spectra from (a) ZrC, (b) ZrN, (c) HfC, and (d) HfN thin film samples. In each case result after etching with 0.5, 1, and 4 keV Ar^+ ions are shown. To facilitate comparison, spectra are normalized to the intensity of corresponding 3d (for ZrC and ZrN) or 4f (for HfC and HfN) metal lines.

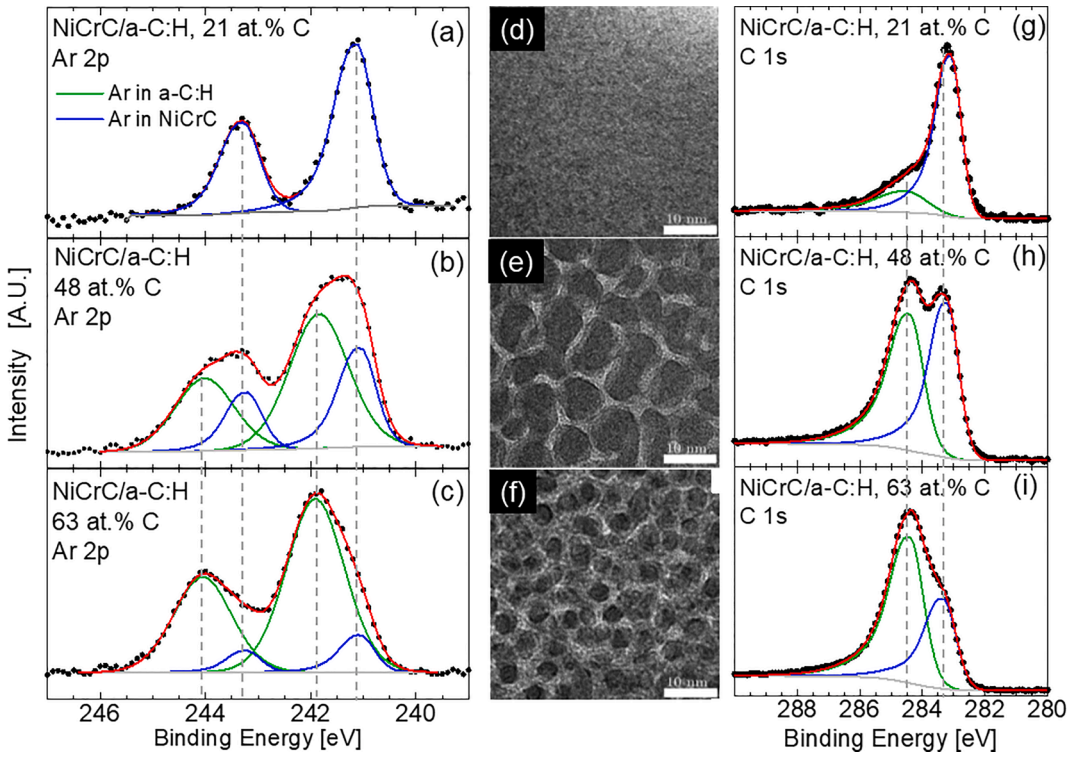

Fig. 11. Ar 2p spectra recorded after 10 min. sputter-etching with 0.5 keV Ar^+ ions incident at an angle of 70° from the surface normal from NiCrC/a-C:H thin film samples containing (a) 21, (b) 48, and (c) 63 at.% C. (d) cross-sectional TEM image of the sample containing 21 at.% C, showing homogenous nature of the sample over its thickness, (e)-(f) plan view TEM images from samples containing 48, and 63 at.% C, respectively [62]. C 1 s spectra from NiCrC/a-C:H thin film samples containing (g) 21, (h) 48, and (i) 63 at.% C.

sample (which does not exhibit the FL) the Si 2p peak is aligned to the corresponding signal in the nanocomposite $Ti_{0.74}Si_{0.26}N$ film. Corresponding survey and major core level spectra are shown in the Supplementary file. The two-phase nanostructure of the nanocomposite $Ti_{0.74}Si_{0.26}N$ film is revealed by the bright-field XTEM image in Fig. 12 (e) together with insets of plan-view STEM micrograph and plan-view EDX/STEM elemental maps. The single-phase nature of the cubic-structure $Ti_{0.76}Si_{0.24}N$ film is proven by cross-sectional STEM micrograph in Fig. 12(f) which includes an HRSTEM lattice-resolved image, as well as by cross-sectional EDX Ti, Si, and N elemental maps (Fig. 12(g)-(j), respectively) together with Ti and Si elemental EDX maps superimposed on the STEM image (Fig. 12(k)).

The Ar 2p spectrum from the reference TiN film is composed of two doublets, as discussed in detail in Sec. 3.3, and dominated by the low BE signal with the Ar $2p_{3/2}$ peak at 243.1 eV. The Ar 2p spectrum recorded from the nanocomposite sample (Fig. 12(b)) can be fitted with two doublets: one corresponding to Ar in TiN crystallites (with the Ar $2p_{3/2}$ peak at 243.1 eV, i.e., exactly matching the peak positions in the reference TiN film) and one shifted to lower BE (with the Ar $2p_{3/2}$ peak at 241.8 eV) assigned to Ar incorporated in the SiN_x phase. Interestingly, in the case of a single-phase film (see Fig. 12(c)) only one pair of Ar peaks is detected with the Ar $2p_{3/2}$ at 242.1 eV, i.e., the value that is between that of cubic TiN and amorphous SiN_x. Finally, the Ar $2p_{3/2}$ peak of the reference SiN film is at 241.7 eV (Fig. 12(d)), i.e., it matches the Ar $2p_{3/2}$ signal from the SiN tissue phase of the nanocomposite sample.

Both examples presented in this section reveal further complications with the charge referencing method based on the Ar 2p signal. The presence of multiple doublets, demonstrated here for NiCrC/a-C:H and TiSiN films and very likely the case for other inhomogeneous samples, introduces additional uncertainty as to which Ar $2p_{3/2}$ peak should be used for referencing. This issue is essential as many technologically-relevant materials nowadays have multiphase structure.

3.5. Factors affecting the Ar 2p peak positions

There are obviously several reasons for the Ar $2p_{3/2}$ peak shifts described in Sections 3.2-3.4. Below we sort out factors that need to be considered for eventual detailed analysis.

1. The screening effect, i.e., relaxation of the surrounding host matrix electron cloud to the lower energy state in response to the core hole creation (also called core hole screening or polarization energy). Screening is sometimes divided into intra-atomic (relaxation of the ionized atom wavefunctions around the core hole) and extra-atomic (response of the medium surrounding the ionized atom) contributions [21,65,66]. The extra energy is carried away by the core electron that leaves the system, resulting in the lower core level BE as compared to that measured for the same atom in the gas phase.
2. For chemically homogenous samples, implanted Ar can reside at different sites. For example, Ar can be found as an interstitial in the crystalline grains, segregate at grain boundaries [33,67], reside in amorphous regions of two-phase samples,[68] or even form gas bubbles [69]. The latter topic is a subject of an extensive research due to intriguing properties of such noble gas bubbles entrapped in solid samples [70–72]. Depending on bubble size, Gibbs-Thomson capillarity force may lead to liquid or solid phase of the inert element.
3. For Ar present as gas bubbles the BE of Ar 2p varies with the bubble size [51–53]. The radius of bubbles is inversely proportional to the pressure [73], which allows to explain the changes in Ar BE by compression of electron wave functions [53].
4. Ar irradiation is destructive to most materials, meaning that implanted Ar cannot be accommodated in the host matrix [74]. Sputter damage, in particular sputter reduction of oxides and other delicate compounds, means that the usefulness of

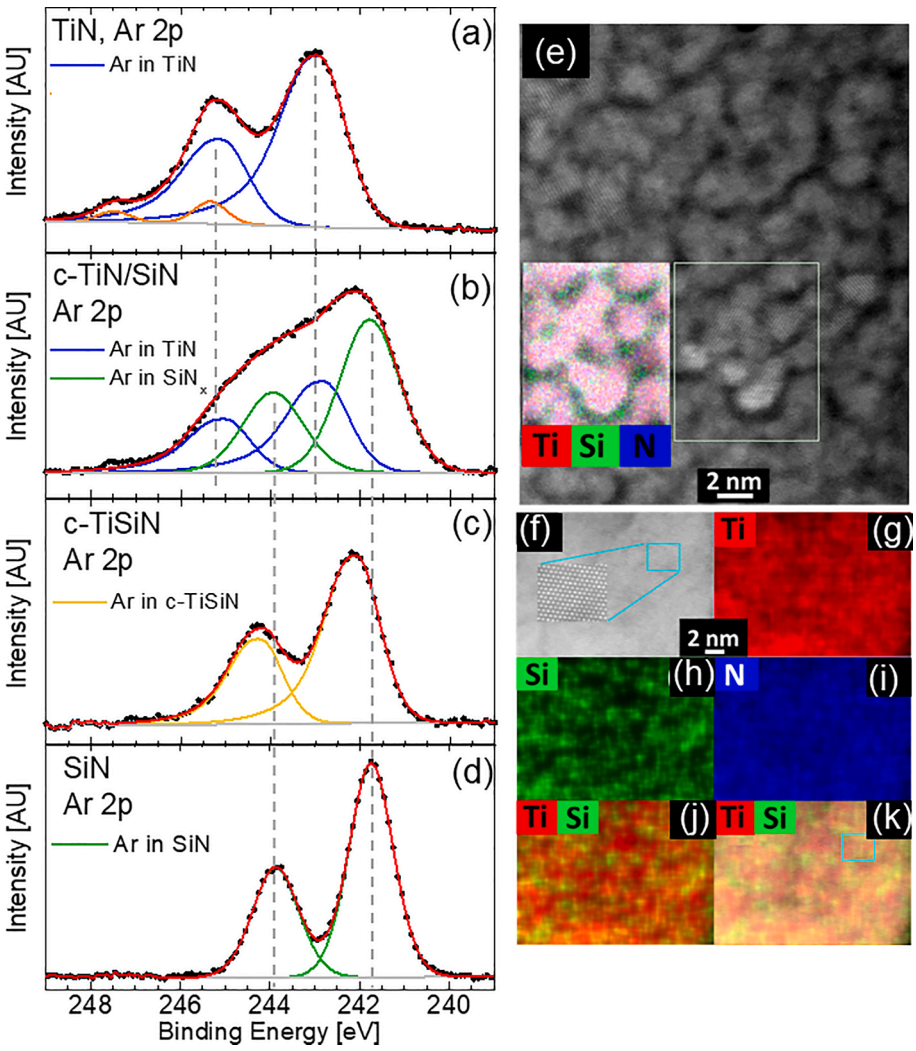

Fig. 12. Ar 2p spectra acquired after sputter-etching with 4 keV Ar^+ ions incident at an angle of 20° from the surface plane from: (a) a reference single-phase cubic TiN film, (b) a nanocomposite $Ti_{0.74}Si_{0.26}N$ film consisting of cubic-structure TiN-rich crystallites embedded in the SiN_x tissue phase, (c) single-phase cubic-structure $Ti_{0.76}Si_{0.24}N$ film, and (d) a reference SiN film. (e) a plan-view STEM micrograph and a plan-view EDX/STEM elemental maps showing Ti (red), Si (green), and N (blue) spatial distributions, acquired from the outlined area of the $Ti_{0.74}Si_{0.26}N$ film. (f) cross-sectional STEM micrograph of a $Ti_{0.76}Si_{0.24}N$ film including an HRSTEM lattice-resolved image, (g)-(j) cross-sectional EDX elemental maps showing Ti (red), Si (green), and N (blue) spatial distributions, and (k) Ti and Si elemental EDX maps together with the STEM image [64].

implantation of Ar for a charge reference may be entirely negated by the change in chemistries/reduction/damage at the sample surface.

5. Sputter damage is a function of the Ar^+ incident energy. Higher Ar^+ energy implies that (i) the thickness of the top layer modified by Ar beam increases and becomes comparable to the XPS probing depth [75], (ii) the sputter damage effects increase [25]. Thus, the position of Ar 2p peaks will depend on the specific conditions (ion energy, incidence angle, fluence) used for Ar implantation.
6. For polycrystalline single-phase compounds Ar ions can channel to different depth with variable end state in differently-oriented grains, which can result in confusing Ar 2p spectra from such samples.
7. Ar atom core energy levels can be affected by the neighboring atoms. This is because the implanted atom's outer electron wave functions are compressed leading to an increased Coulomb interaction between valence and core electrons, and, in consequence, lowered core level BEs [21].
8. Since Ar is a noble element, it is commonly not considered to chemically bond. Yet, it binds weakly to some other atoms like H, C, or B and form Van der Waals molecules [54–56], which means that Ar 2p chemical shifts should not be *a priori* excluded.
9. For thin films, internal stress state can affect XPS peak positions of implanted noble gas atoms – compression leads to gas clustering and bubble formation. Shifts up to 1 eV to lower BE for Ar implanted in carbon films with different stress levels (up to 11 GPa) have thus been reported [63]. It was proposed that the internal pressure affects the outer valence electron wave functions of implanted gas atoms leading to the change of core level BEs (initial state effect). In addition, the extra-atomic relaxation is also affected (the final state effect).
10. For Ar implanted into inhomogeneous samples, the core level BEs may vary depending where (in which phase) the photoemission takes place, especially if phases have different electrical conductivity (see examples in Sec. 3.4).

4. Summary and conclusions

The reliability of using Ar $2p_{3/2}$ peak of implanted Ar for charge referencing XPS spectra is critically evaluated for thin film samples of differing composition among metals and ceramics. All selected specimens possess a well-defined Fermi edge, which serves as an independent internal reference, hence potential complications due to charging can be excluded. The method of Ar $2p_{3/2}$ referencing was proposed 40 years ago and relies upon the assumption that the core level BE of inert gas atoms is only affected by the local electrical potential, hence, it could serve the purpose of charge reference. The advantage over the C 1 s/AdC method would be that the reference signal comes from an element implanted in the sample of interest (and not present in an external layer such as AdC) and that Ar is implanted in samples during sputter etching (when AdC is removed). The "correct" BE of the Ar $2p_{3/2}$ line was established at

241.5 ± 0.2 eV for metallic samples and 242.3 eV for insulators.

Our evaluation shows that the BE of the Ar $2p_{3/2}$ peak varies by as much as 5.1 eV with respect to the sample Fermi level (if referenced to the sample VL the variation is 4.0 eV). *Such large peak shifts between various sample types clearly disqualifies Ar $2p_{3/2}$ peak as a charge reference.* The largest deviation from the "reference" value to the low BE side is 1.2 eV for Pt film, while the largest deviation to the high BE side is 3.9 eV for TiN.

The BE of the Ar 2p peaks shows a strong correlation to the number of valence electrons available for screening, implying that the polarization energy has a significant role for the observed large spread of Ar $2p_{3/2}$ BE values.

For several thin film samples, two Ar 2p doublets are observed (although the thin film specimens are homogenous single-phase materials) with the higher BE pair being shifted to very high energy values. If referenced to the sample vacuum level, the Ar $2p_{3/2}$ BE for TiN, HfC, ZrC, TiC, and NbC samples is higher than the gas phase value of 248.6 eV [10]. To the best of our knowledge this is the first time such high BE values are reported for Ar implanted in solid state samples. All observations allow us to exclude the possibility that the high BE peaks are due to Ar interstitials or bubbles. Instead, we tentatively assign them to the formation of Ar-C and possibly also Ar-N complexes stabilized by the Van der Waals forces.

Ar implantation into inhomogeneous two-phase samples results in complex Ar 2p spectra with the area ratio between two spin-split doublets determined by the volume ratio of co-existing phases together with Ar concentration in each phase, while the BE splitting depends primarily on how both phases respond to the core hole creation. This introduces additional uncertainty as to how (if at all) Ar $2p_{3/2}$ signal should be used for spectra referencing.

The firm conclusion from our broad systematic study is that the Ar $2p_{3/2}$ peak from implanted Ar is not a remedy for the charge referencing problem. The position of this peak varies by as much as 5.1 eV depending on the sample, which is more than typical chemical shifts. This excludes any meaningful determination of chemical bonding. In fact, the Ar 2p method is even less reliable than the one using adventitious carbon, as the BE spread is almost twice larger in the former case. Thus, the use of Ar $2p_{3/2}$ peak for charge referencing should be terminated.

CRediT authorship contribution statement

G. Greczynski: Conceptualization, Investigation, Funding acquisition, Writing – original draft. **L. Hultman:** Writing – review & editing, Funding acquisition.

Declaration of Competing Interest

The authors declare that they have no known competing financial interests or personal relationships that could have appeared to influence the work reported in this paper.

Acknowledgements

The authors acknowledge financial support of the Swedish Research Council VR Grant 2018-03957, the Swedish Energy Agency under project 51201-1, the Knut and Alice Wallenberg Foundation Scholar Grant KAW2019.0290, the Åforsk Foundation Grant 22-4, the Carl Tryggers Stiftelse contract CTS 20:150, and the Swedish Government Strategic Research Area in Materials Science on Advanced Functional Materials at Linköping University (Faculty Grant SFO-Mat-LiU No. 2009-00971).

Appendix A. Supplementary data

Supplementary data to this article can be found online at https://doi.org/10.1016/j.apsusc.2023.157598.

References

[1] K. Siegbahn, C. Nordling, ESCA, atomic, molecular and solid state structure studied by means of electron spectroscopy. Nov. Act. Uppsaliensis. 1967.
[2] E. Sokolowski, C. Nordling, K. Siegbahn, Chemical shift effect in inner electronic levels of Cu due to oxidation, Phys. Rev. 110 (1958) 776.
[3] S. Hagström, C. Nordling, K. Siegbahn, Electron spectroscopy for chemical analyses, Phys. Lett. 9 (1964) 235–236.
[4] K. Asami, J. Nectron Spectrosc. 9 (1976) 469.
[5] K. Richter, B. Peplinski, J. Electron Spectrosc. 13 (1978) 69.
[6] R.J. Bird, P. Swift, J. Electron Spectrosc. 21 (1980) 227.
[7] M.T. Anthony, M.P. Seah, Surf. Interf. Anal. 6 (1984) 95.
[8] J. Cazaux, J. El. Spectr. Rel. Phenom. 105 (1999) 155.
[9] D.J. Hnatowich, J. Hudis, M.L. Perlman, R.C. Ragaini, Determination of charging effect in photoelectron spectroscopy of nonconducting solids, J. Appl. Phys. 42 (1971) 4883–4886.
[10] G. Johansson, J. Hedman, A. Berndtsson, M. Klasson, R. Nilsson, Calibration of electron spectra, J. Electron Spectrosc. 2 (1973) 295.
[11] R. Nordberg, H. Brecht, R.G. Albridge, A. Fahlman, J.R. Van Wazer, Binding energy of the" 2p" electrons of silicon in various compounds, Inorg. Chem. 9 (1970) 2469–2474.
[12] S. Kinoshita, T. Ohta, H. Kuroda, Comments on the Energy Calibration in X-ray Photoelectron Spectroscopy, Bull. Chem. Soc. Jpn. 49 (1976) 1149–1150.
[13] W.P. Dianis, J.E. Lester, External standards in X-ray photoelectron spectroscopy. Comparison of gold, carbon, and molybdenum trioxide, Anal. Chem. 45 (1973) 1416–1420.
[14] P. Swift, Adventitious carbon—the panacea for energy referencing? Surf. Interf. Anal. 4 (1982) 47–51.
[15] G. Greczynski, L. Hultman, ChemPhysChem 18 (2017) 1507.
[16] G. Greczynski, L. Hultman, Prog. Mater Sci. 107 (2020), 100591.
[17] P.J.K. Paterson, P.H. Holloway, Y.E. Strausser, Appl. Surf. Sci. 4 (1980) 37.
[18] S. Kohiki, T. Ohmura, K. Kusao, J. Electron Spectr. Rel. Phenom. 28 (1983) 229.
[19] S. Kohiki, T. Ohmura, K. Kusao, J. Electron Spectr. Rel. Phenom. 31 (1983) 85.
[20] P.H. Citrin, D.R. Hamann, Phys. Rev. B 10 (1974) 4948.
[21] R.E. Watson, J.F. Herbst, J.W. Wilkins, Phys. Rev. B 14 (1976) 18.
[22] B.J. Waclawski, J.W. Gadzuk, J.F. Herbst, Phys. Rev. Lett. 41 (1978) 583.
[23] E. Lewin, J. Counsell, J. Patscheider, Spectral artefacts post sputter-etching and how to cope with them – a case study of XPS on nitride-based coatings using monoatomic and cluster ion beams, Appl. Surf. Sci. 442 (2018) 487.
[24] R. Steinberger, et al., XPS study of the effects of long-term Ar+ ion and Ar cluster sputtering on the chemical degradation of hydrozincite and iron oxide, Corros. Sci. 99 (2015) 66–75.
[25] G. Greczynski, L. Hultman, Appl. Surf. Sci. 542 (2021), 148599.
[26] L.B. Church, J. Lyngdal, J. Electron Spectr. Rel. Phenom. 41 (1986) 89.
[27] A.E. Hughes, B.A. Sexton, J. Electron Spectr. Rel. Phenom. 50 (1990), c15.
[28] S. Kohiki, K. Oki, J. Electron Spectr. Rel. Phenom. 36 (1984) 105.
[29] S. Kohiki, Applications of Surface Science 17 (1984) 497.
[30] S.B. DiCenzo, S.D. Berry, E.H. Hartford Jr, Photoelectron spectroscopy of single-size Au clusters collected on a substrate, Phys. Rev. B 38 (1988) 8465.
[31] G.K. Wertheim, S.B. DiCenzo, S.E. Youngquist, Unit charge on supported gold clusters in photoemission final state, Phys. Rev. Lett. 51 (1983) 2310.
[32] G. Greczynski, L. Hultman, Appl. Surf. Sci. 606 (2022), 154855.
[33] A. Pélisson-Schecker, H.J. Hug, J. Patscheider, Surface and Interface, Analysis 44 (2012) 29.
[34] E. Watanabe, M. Yoshinari, Appl. Phys. A 122 (2016) 1.
[35] J. Werckmann, P. Humbert, C. Esnouf, J.C. Broudic, S. Vilminot, J. Mat. Sci. 28 (1993) 5229.
[36] H. Lu, C.L. Bao, D.H. Shen, J. Qin, Y.D. Cui, Y.X. Wang, J. Phys. Chem. of Solids 58 (1997) 257.
[37] G.M. Ingo, L. Giorgi, N. Zacchetti, N. Azzerri, Corros. Sci. 33 (1992) 361.
[38] T. Hagio, A. Takase, S. Umebayashi, J. Mat. Sci. Letters 11 (1992) 878.
[39] P. Humbert, J.P. Deville, J. Phys. C: Solid State Physics 20 (1987) 4679.
[40] A. Hiraki, M.-A. Nicalet, J.W. Mayer, Appl. Phys. Lett. 18 (1971) 178.
[41] A. Cros, J. Derrien, F. Salvan, Surf. Sci. 110 (1981) 471.
[42] J.T. Robinson, P.G. Evans, J.A. Liddle, O.D. Dubon, Nano Lett. 7 (2007) 2009.
[43] G. Greczynski, S. Mráz, L. Hultman, J.M. Schneider, Appl. Phys. Lett. 108 (2016), 041603.
[44] ISO 15472, Surface chemical analysis- x-ray photoelectron spectrometers - calibration of energy scales (ISO, Geneva, 2001).
[45] J.F. Moulder, W.F. Stickle, P.E. Sobol, K.D. Bomben, Handbook of X-rayPhotoelectron Spectroscopy, Perkin-Elmer Corporation, Eden Prairie, USA.
[46] N. Fairley, V. Fernandez, M. Richard-Plouet, C. Guillot-Deudon, J. Walton, E. Smith, D. Flahaut, et al., Applied Surface Science Advances 5 (2021), 100112.
[47] G.H. Major, N. Fairley, P.M.A. Sherwood, M.R. Linford, J. Terry, V. Fernandez, K. Artyushkova, J. Vac. Sci. Technol. 38 (2020), 061203.
[48] see for example: Chapter 1 in S. Hűfner Photoelectron Spectroscopy: Principles and Applications, 3rd Ed. Springer 2003, ISSN 1439-2674.
[49] H. Ishii, E. Sugiyama, E. Ito, K. Seki, Adv. Mat. 11 (1999) 605.
[50] A.R. Lahrood, T. de Los Arcos, M. Prenzel, A. von Keudell, J. Winter, Thin Solid Films 520 (2011) 1625.
[51] C. Biswas, A.K. Shukla, S. Banik, S.R. Barman, A. Chakrabarti, Phys. Rev. Lett. 92 (2004), 115506.
[52] R.S. Dhaka, S.R. Barman, Surf. Coat. Technol. 203 (2009) 2380.

[53] R.S. Dhaka, C. Biswas, A.K. Shukla, S.R. Barman, Phys. Rev. B 77 (2008), 104119.
[54] B.L. Blaney, G.E. Ewing, Van Der Waals Molecules, Annu. Rev. Phys. Chem. 27 (1) (1976) 553–584.
[55] J. Lei, P.J. Dagdigian, Laser fluorescence excitation spectroscopy of the CAr van der Waals complex, J. Chem. Phys. 113 (2) (2000) 602.
[56] X. Yang, P.J. Dagdigian, Fluorescence excitation and depletion spectroscopy of the BAr complex: Electronic states correlating with the excited valence B(2s2p2 2D) asymptote, J. Chem. Phys. 106 (16) (1997) 6596.
[57] L. Porte, L. Roux, J. Hanus, Vacancy effects in the x-ray photoelectron spectra of TiN_x, Phys. Rev. B. 28 (1983) 3214.
[58] I. Strydom, S. Hofmann, The contribution of characteristic energy losses in the core-level X-ray photoelectron spectroscopy peaks of TiN and (Ti, Al) N studied by electron energy loss spectroscopy and X-ray photoelectron spectroscopy, J. Electron Spectrosc. Relat. Phenom. 56 (1991) 85.
[59] A. Arranz, C. Palacio, Screening effects in the Ti 2p core level spectra of Ti-based ternary nitrides, Surf. Sci. 600 (2006) 2510.
[60] G. Greczynski, L. Hultman, Appl. Surf. Sci. 396 (2017) 347–358.
[61] E. Lewin, P.O.Å. Persson, M. Lattemann, M. Stüber, M. Gorgoi, A. Sandell, C. Ziebert, et al., On the origin of a third spectral component of C1s XPS-spectra for nc-TiC/aC nanocomposite thin films, Surf. Coat. Technol. 202 (2008) 3563–3570.
[62] T. Suszko, W. Gulbiński, K. Załęski, G. Greczynski, J. Morgiel, V. Lapitskaya, Appl. Surf. Sci. 591 (2022), 153134.
[63] R.G. Lacerda, M.C. Dos Santos, L.R. Tessler, P. Hammer, F. Alvarez, F.C. Marques, Phys. Rev. B 68 (2003), 054104.
[64] G. Greczynski, J. Patscheider, J. Lu, B. Alling, A. Ektarawong, J. Jensen, I. Petrov, J.E. Greene, L. Hultman, Surf. Coat. Technol. 280 (2015) 174.
[65] J.W. Gadzuk, Phys. Rev. B 14 (1976) 2267.
[66] D.A. Shirley, Chem. Phys. Lett. 16 (1972) 220.
[67] D. Magnfält, G. Abadias, K. Sarakinos, Appl. Phys. Lett. 103 (2013), 051910.
[68] M. Prenzel, T. de los Arcos, A. Kortmann, J. Winter, A. von Keudell, *J. App. Phys.* 112 (2012) 103306.
[69] C.J. Rossouw, S.E. Donnelly, Phys. Rev. Lett. 55 (1985) 2960.
[70] S. Kakar, O. Björneholm, J. Weigelt, A.R.B. De Castro, L. Tröger, R. Frahm, T. Möller, A. Knop, E. Rühl, Phys. Rev. Lett. 78 (1997) 1675.
[71] A. Knop, B. Wassermann, E. Rühl, Phys. Rev. Lett. 80 (1998) 2302.
[72] F. Federmann, O. Björneholm, A. Beutler, T. Möller, Phys. Rev. Lett. 73 (1994) 1549.
[73] J. Fink, Adv. Electron. Electron Phys. 75 (1989) 121.
[74] J.S. Pan, A.T.S. Wee, C.H.A. Huan, H.S. Tan, K.L. Tan, J. Appl. Phys. 79 (1996) 2934.
[75] G. Greczynski, L. Hultman, J. Appl. Phys. 132 (2022), 011101.